

Extraction of ionization spectra from correlated wave functions: a comparison between different methods

Luca Argenti^{1,*}, Renate Pazourek², Johannes Feist³, Stefan Nagele²,

Matthias Liertz², Emil Persson², Joachim Burgdörfer², and Eva Lindroth⁴

¹*Departamento de Química, Módulo 13, Universidad Autónoma de Madrid, 28049 Madrid, Spain, EU*

²*Institute for Theoretical Physics, Vienna University of Technology, 1040 Vienna, Austria, EU*

³*ITAMP, Harvard-Smithsonian Center for Astrophysics, Cambridge, Massachusetts 02138, USA and*

⁴*Department of Physics, Stockholm University, AlbaNova University Center, SE-106 91 Stockholm, Sweden, EU*

(Dated: September 13, 2022)

We compare three techniques to extract partial photoelectron spectra from the wave packet resulting from the integration on a finite-element discrete variable representation basis of the time-dependent Schrödinger equation for an helium atom subject to an ultra-short XUV pulse. These techniques are: projection on products of hydrogenic bound and continuum states, projection onto multi-channel scattering states computed in a B-spline close-coupling basis, and a technique based on exterior complex scaling (ECS) [Palacios *et al*, Phys. Rev. A **76**, 043420 (2007)] implemented in the same basis used for the time propagation. These methods allow to monitor the population of continuum states in wave packets created with ultrashort pulses in different regimes. The first method works well at the energies where the ionization continuum is unstructured while it becomes inefficient close to threshold openings due to the presence of long-lived metastable states or of vanishingly slow photofragments. The agreement between the last two methods is excellent below the double ionization threshold. This result shows that in regions where the projection on Coulomb functions is inapplicable, scattering states computed in an optimized basis can be converted to a representation well suited to time-dependent simulations. Above the double ionization threshold, the projection onto Coulomb functions and the ECS method are found in excellent agreement with each other.

PACS numbers: 31.15.ac, 32.80.Fb, 32.80.Rm, 32.80.Zb

I. INTRODUCTION

During the last decade, two transformational experimental techniques, high harmonic generation [1] and x-ray free electron lasers [2], have given access to femtosecond and sub-femtosecond intense light pulses in the XUV and soft x-ray energy range, thus opening the way to time resolved studies of the correlated motion of electrons in atoms and molecules on their characteristic time-scale [3–10]. These new techniques can be used not only to monitor the electronic motion but also to steer it [11, 12]. This latter capability offers the perspective of controlling dynamics at the femtosecond and sub-femtosecond timescale, such as electronic dynamics in atoms [13, 14], molecules [15–17], and solids [18], and eventually also nuclear dynamics such as fast proton migration [19].

The interpretation of experiments on attosecond dynamics, however, face a number of difficulties and require guidance by theory. First, sub-femtosecond pulses typically excite the target to a coherent superposition of states above the ionization threshold and across a wide range of energies. As a consequence, several different ionization regimes such as multiply excited autoionizing states, multichannel single ionization states and, possibly, multiple ionization states, are accessed at the same time. Second, in common pump-probe schemes [15], the

strong few-cycle IR-probe pulse that follows an attosecond weak XUV-pump pulse gives rise to electronic dynamics that unfolds on a very short time-scale through non-perturbative stages, e.g. tunneling, over-the-barrier ionization, and Rabi oscillations.

Traditional perturbative approaches [20] are clearly not well suited to describe such dynamical regimes. Moreover, since the duration of compressed IR pulses easily spans just a few [21] or even a single [22] carrier cycle, stationary non-perturbative techniques like those based on the Floquet method [23] cannot be used either. Reliable theoretical predictions for ultrashort processes, therefore, generally require direct integration of the time-dependent Schrödinger equation (TDSE) [14, 24–34]. Such an approach permits to reproduce faithfully the physical process under study. However, it gives rise to a multitude of problems as well. Relevant parts, if not most, of the electron dynamics triggered by sub-femtosecond pulses take place in the ionization continuum. Indeed, typical experiments are designed to monitor the energy and angular distribution of the photoelectrons emerging from the reaction center, e.g., with a velocity map imaging spectrometer [35] or even several photo-fragments in coincidence, e.g., with a reaction microscope [36]. Transient absorption spectroscopy [37], which monitors quasi-bound electronic dynamics, constitutes a notable exception. One of the most prominent problems theory has to face is then how to extract from a numerical simulation, intrinsically limited in both time and space, the relevant asymptotic scattering informa-

* luca.argenti@uam.es

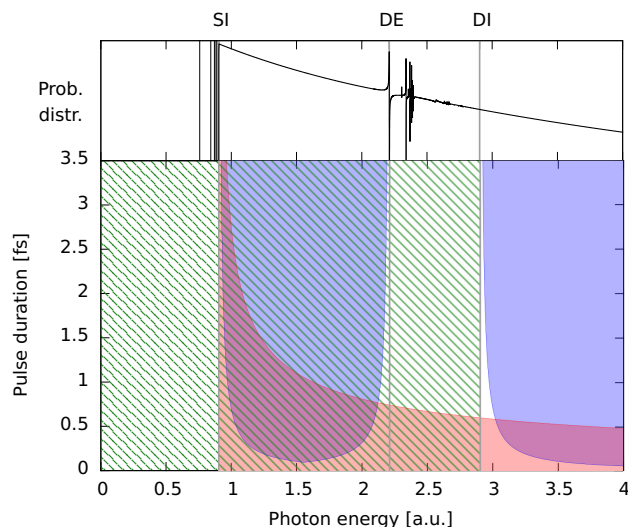


FIG. 1. Approximate regions of applicability of different extraction methods for the single ionization continuum of helium as a function of photon energy and pulse duration for a single-photon transition. SI: single ionization, DE: double excitation, DI: double ionization. Green shaded: projection on scattering states, blue solid: projection on products of Coulomb functions, red solid: Berkeley ECS method. See text for details. The upper part shows the (logarithmic) ionization probability for single ionization and positions of excited bound states.

tion.

A number of alternative techniques have been used in the past to extract differential distributions of the products of a light-induced reaction from an entangled wave function: spectral analysis of autocorrelation functions [38], analysis of the radial flux at large distances [39], projection of the wave packet onto products of one-particle functions, e.g., Coulomb functions [26, 32, 40] or Volkov states [28], surface integration of the monochromatic component of the wave function extracted with a technique based on exterior complex scaling (Berkeley-ECS) [41, 42], or projection on scattering states computed on the same basis used to carry out the time propagation [14, 29–31, 40, 43, 44].

In the following, we compare three of these techniques in more detail for the prototypical three-body system, the helium atom: projection on products of one-particle functions, projection on scattering states, and the Berkeley-ECS method. For all these techniques, the extraction of asymptotic scattering information takes place in the field-free region after the laser pulse is over. As will be discussed in more detail later, each of these approaches has its strengths and drawbacks making it applicable for different photon energies and pulse durations. These regions are schematically illustrated in Fig. 1.

We here give a brief preview. The projection on products of Coulomb functions works well when the wave packet only contains electrons that are already

well-separated in radial space. While this is relatively straightforward to achieve at high energies (such as above the double ionization continuum), it becomes prohibitive close to the doubly excited resonances that populate the energy region from around -0.7 a.u. to 0 a.u., and which only decay after many femtoseconds. The main advantages of this approach are its analytical and numerical simplicity and the fact that it works above the double ionization threshold. This allows it to be used even when very large computational boxes are employed, and consequently with very long driving pulses. In the case of single ionization, a closely related approach with almost identical properties is the projection on *channel functions*, i.e., eigenstates obtained by freezing the inner electron in an ionic state.

Projection on scattering states (PSS), on the other hand, works for any separation of the final particles, and thus can be used also when doubly excited resonances are excited and before they have decayed. The algorithms to calculate atomic and molecular scattering states have now achieved a considerable level of sophistication and can be used with large radial boxes, i.e., for large separation of the electrons. Moreover, the calculation of scattering states is independent of the actual simulation and can be optimized separately. Yet, scattering states have so far been employed only in those cases where they are built in the same basis which is used to carry out the simulations. We demonstrate below that the scattering states computed in an optimized B-spline close-coupling basis with the K-matrix method [45] can be accurately converted to a finite-element discrete-variable (FEDVR) basis [32] optimized for time propagation. Fully differential photoelectron spectra can thus be extracted from the wave packet arising in photoionization by means of a simple projection. However, scattering states are not available above the double ionization threshold as the boundary conditions for double ionization [46] cannot be easily enforced due to the infinite set of constraints they entail (as opposed to the finite number of constraints of single ionization problems). In addition, the scattering states become exceedingly expensive to calculate as the double ionization threshold is approached from below due to the presence of many double Rydberg series.

Finally, the Berkeley ECS method is applicable for both single and double ionization, and also works when resonances and other long-lived states are involved. Its main drawback is the computational complexity: for each desired final energy, a large linear system representing the exterior-complex-scaled Hamiltonian acting on the final wave packet has to be iteratively solved. This approach becomes computationally expensive when the system has large spatial extent and when the wave packet to be analyzed covers a wide range of energies. With currently available supercomputers, this becomes impractical for linear systems with a dimension of more than a few million. For typical simulations in helium this limits the box sizes to the range of $\sim r_{max} = 250$ a.u. and thus to simulations where only relatively short pulses are used.

For the comparison of the methods, we choose the pulse parameters to highlight the limitations of the “most straightforward” projection methods, the projection on the product of Coulomb functions or similar single-channel functions. These limitations emerge most markedly when autoionizing states are excited, in which case convergence cannot be achieved. Such behavior is to be contrasted with the Berkeley-ECS method and the projection on scattering states which yield convergent results in excellent agreement with each other. We demonstrate that scattering states can be fruitfully ported across different bases, thus giving access to a numerically convenient and accurate method of monitoring the single ionization component of a wave packet below the double ionization threshold.

The article is organized as follows. In section II we introduce the different approaches that are used in this work to extract physical information from a wave packet and put them in comparison from a theoretical perspective. In section III we briefly summarize the propagation method for the time dependent wave function in the finite-element discrete-variable representation. In section IV we illustrate the details of the methods for extracting information from the time-dependent wave packet. In section V we present simulation results highlighting the similarities and differences between different extraction methods. Finally, in section VI we draw our conclusions.

II. THEORETICAL PRELIMINARIES

The electronic dynamics induced in an atom or molecule by attosecond pulses is encoded in the energy and angular distribution of the emergent photofragments. To unravel the mechanism underlying the break-up process it is thus necessary to establish a correspondence between these experimental observables and the simulated wave packet dynamics. In principle, this is straightforward: since the photofragments are collected at macroscopic distances from the reaction center, the final kinematic state of the system is fully identified by a complete set of quantum numbers for the separated fragments. In practice, however, several complications arise which we briefly review in the following. Upon conclusion of the electromagnetic pulse, the numerical solution of the TDSE yields the wave function $\Psi(t)$ of the wave packet. The dynamics of $\Psi(t)$ is then governed by the total field-free atomic Hamiltonian, H_a . The state $\Psi(t)$ is composed of a bound and an unbound part. Let us indicate by Λ the projector on the bound states of H_a , and with $\Psi'(t) = (\mathbb{1} - \Lambda)\Psi(t)$ the unbound part of $\Psi(t)$. The fragments detected are associated with the long-time limit of the unbound component $\Psi'(t)$. It consists of a superposition of unbound eigenstates $\varphi_{\alpha\epsilon}$ of the sum of the Hamiltonians of the separated fragments, H_0 . In mathematical terms the latter is frequently referred to as

asymptotic completeness [47, 48]

$$\lim_{t \rightarrow \infty} \left\| \Psi'(t) - e^{-iH_0 t} \sum_{\alpha} \int d\epsilon \varphi_{\alpha\epsilon} c_{\alpha\epsilon}(t) \right\| = 0, \quad (1)$$

where

$$c_{\alpha\epsilon}(t) = \langle \varphi_{\alpha\epsilon} | \Psi'(t) \rangle e^{i\epsilon t}. \quad (2)$$

In Eqs. (1,2), α designates the collective set of quantum numbers beyond the total energy identifying uniquely the final state of the system. These include the fragmentation channel of the target, the asymptotic angular distribution of the photofragments, and their internal quantum numbers (e.g. spin and angular momentum).

The expansion coefficients $c_{\alpha\epsilon}(t)$ in (1) may not necessarily converge in the infinite-time limit. In particular, when two or more fragments are charged, the phase of $c_{\alpha\epsilon}(t)$ diverges due to the long-range character of the Coulomb field. Notwithstanding this difficulty the probability density $|c_{\alpha\epsilon}(t)|^2$ will still converge in the sense of distributions (i.e., when convoluted with a test function) yielding a well defined asymptotic distribution of the fragments.

In the case of two charged fragments, a stronger result is known to hold: the absolute value $|c_{\alpha\epsilon}(t)|$ itself converges [48] as $t \rightarrow \infty$. Hence, the probability distribution $P_{\alpha}(E)$ for the detection of fragments in channel α and with energy E at the end of the propagation is given by

$$P_{\alpha}(E) = \lim_{t \rightarrow \infty} |c_{\alpha E}(t)|^2. \quad (3)$$

More details on this result can be found in Sec. XI.9 of [48]. Moreover, a substantial body of numerical evidence [30, 34, 40, 49, 50] indicates that the more lenient result (3) holds in the case of atomic double photoionization as well.

For the time being we will thus assume that, with suitable precautions, Eq. 3 is applicable. The probability distribution $P_{\alpha}(E)$ can then be computed as

$$P_{\alpha}(E) = \lim_{t \rightarrow \infty} |\langle \varphi_{\alpha E} | \mathbb{1} - \Lambda | \Psi(t) \rangle|^2. \quad (4)$$

At first sight, the prescription (4) to extract experimental observables from a wave packet has the appeal of simplicity since the uncoupled states $\varphi_{\alpha E}$ are usually more easily obtainable than the continuum eigenstates of the full Hamiltonian. This simplicity, though, is misleading since the projector Λ of the total Hamiltonian requires at least a certain number of bound states of the fully interacting system to be known. Since the bound states of H_a are not orthogonal to $\varphi_{\alpha E}$, their elimination is essential. Otherwise they would give rise to spurious contributions to the ionization channels which do not vanish for large times.

The greatest drawback of Eq. 4, however, stems from the asymptotic time limit, which may be out of reach for the propagation algorithm. Even by the inclusion of part of the long-range interactions between photofragments

into the reference Hamiltonian H_0 this problem can only be marginally alleviated rather than solved. More generally, all the methods that require the wave packet to reach the asymptotic region, i.e. the region where the dynamics governed by H_0 and H_a become equivalent, face the same problem, namely the propagation of the fully correlated wave function for long times and at large distances which may be computationally prohibitively expensive. This limitation becomes particularly severe in a number of circumstances frequently encountered in atomic photoionization. For example, when the wave packet spectrum is distributed across an ionization threshold, the wave packet comprises components with vanishingly small kinetic energy that take exceedingly long times to reach the asymptotic region. Even more severe, when several channels with different thresholds are simultaneously open, both slow and fast photoelectrons are present at the same time. Hence, in order for the slowest part of the wave function to reach the asymptotic region, the propagation box must be large enough to accommodate for the fastest components as well. A further difficulty with Eq. 4, perhaps the most relevant in the present context, is provided by resonances in general and by Rydberg series of doubly excited states in particular. Such doubly excited states are a general feature in atomic photoionization spectra. First, the convergence of the resonant profiles in those channels where the excited resonances decay requires a propagation time proportional to the lifetime of the longest lived resonance which is excited in the simulation. Second, doubly excited states have, in general, non-vanishing scalar products with all the eigenfunctions of the unperturbed Hamiltonian, including those belonging to closed ionization channels.

One avenue to circumvent some of the limitations associated with Eq. 4 is to use, instead of the asymptotic states $\varphi_{\alpha E}$, the scattering states $\psi_{\alpha E}^-$ of the total atomic Hamiltonian H_a [47]. The $\psi_{\alpha E}^-$ states fulfill so-called incoming boundary conditions [51, 52], which are appropriate to the context of photoionization, since photoelectrons are observed in the positive time limit.

Such scattering states satisfy the Lippmann-Schwinger equation with advanced Green's functions [47]

$$\psi_{\alpha E}^- = \varphi_{\alpha E} + G_0^-(E)H'\psi_{\alpha E}^- \quad (5)$$

$$= \varphi_{\alpha E} + G^-(E)H'\varphi_{\alpha E} \quad (6)$$

where the operators $G_0^-(E) = (E - H_0 - i0^+)^{-1}$ and $G^-(E) = (E - H_a - i0^+)^{-1}$ are the resolvents of the reference (H_0) and full Hamiltonian (H_a), while $H' = H_a - H_0$ is the corresponding perturbation (the interactions not accounted for by the channel Hamiltonian H_0).

The $\psi_{\alpha E}^-$ states form a complete orthonormal basis for the unbound states of H_a ,

$$H_a\psi_{\alpha E}^- = E\psi_{\alpha E}^-, \quad \langle \psi_{\alpha E}^- | \psi_{\beta E'}^- \rangle = \delta_{\alpha\beta}\delta(E - E') \quad (7)$$

$$1 - \Lambda = \sum_{\alpha} \int d\epsilon |\psi_{\alpha\epsilon}^- \rangle \langle \psi_{\alpha\epsilon}^-|. \quad (8)$$

We can thus write the scattering component $\Psi'(t)$ of the wave packet at any time t after the external field is over as

$$\begin{aligned} |\Psi'(t)\rangle &= e^{-iH_a(t-t_0)}(\mathbb{1} - \Lambda)|\Psi(t_0)\rangle = \\ &= \sum_{\alpha} \int d\epsilon |\psi_{\alpha\epsilon}^- \rangle e^{-i\epsilon(t-t_0)} c_{\alpha\epsilon}^-(t_0) \end{aligned} \quad (9)$$

where

$$c_{\alpha E}^-(t_0) = \langle \psi_{\alpha E}^- | \Psi'(t_0) \rangle. \quad (10)$$

A crucial aspect of equation (9) is that, in the large time limit, the states $\psi_{\alpha\epsilon}^-$ can be replaced by their asymptotes $\varphi_{\alpha\epsilon}$ [51, 52]. This is one defining feature of the ψ^- states, sometimes referred to as control of ψ^- by the future. In particular,

$$\lim_{t \rightarrow \infty} |c_{\alpha\epsilon}(t)| = |c_{\alpha\epsilon}^-(t_0)| \quad (11)$$

To compute the distribution $P_{\alpha}(E)$ we now combine Eq. 3, Eq. 11, and Eq. 10 and obtain the *exact* result

$$P_{\alpha}(E) = |\langle \psi_{\alpha E}^- | \Psi(t_0) \rangle|^2. \quad (12)$$

In contrast to Eq. 4, Eq. 12 requires neither a projection on the bound states of the system, to which the scattering states are orthogonal, nor the evaluation of a long-time limit. The convenience of using scattering states $\psi_{\alpha E}^-$, instead of the asymptotic limits $\varphi_{\alpha E}$, is thus apparent: Eq. 12 can be evaluated as soon as the external time-dependent field is over, without having to wait until the ionizing wave packet reaches the asymptotic region (Eq. 4).

In [40], the use of scattering states has been deemed impractical but in the simplest cases, due to the additional workload required to solve Eq. 5 or Eq. 6. Indeed, no systematic procedure to generate accurate scattering states for the double ionization of atoms has been reported to date. As far as single-ionization processes are concerned, however, the calculation of scattering states is straightforward. This task has been tackled successfully in the course of the last four decades [53–57]. Today several efficient methods capable of computing multi-electron single ionization scattering states are available. They include the R-matrix [58], J-matrix [59], K-matrix [45, 60], Feshbach projection [61], and inverse iteration [62]. Furthermore, the computational overhead for generating scattering states is easily compensated whenever a large number of different simulations must be carried out, as is the case, e.g., of time-delay scans in pump-probe schemes. The biggest drawback of these methods is that they only work for total energies below the double ionization threshold.

A third elegant strategy for computing $P_{\alpha}(E)$, based on exterior complex scaling, was put forward by Palacios, McCurdy and Rescigno [33, 41, 63]. In this approach, referred to in this work as the Berkeley-ECS method, the monochromatic component Ψ_E at energy E of the wave packet $\Psi(t_0)$ is extracted by applying to $\Psi(t_0)$

the retarded resolvent $G^+(E)$ of the total Hamiltonian, $\Psi_E = G^+(E)\Psi(t_0)$, the realization of which in a finite radial domain is provided by the resolvent of an exterior-complex-rotated Hamiltonian H_θ . From the function Ψ_E the distribution of the photofragments is extracted in the asymptotic region. This last step is accomplished [33, 63] by carrying out a surface integral which involves Ψ_E and test functions analogous to the $\varphi_{\alpha E}$ states introduced at the beginning of this section (see Sec. IV).

The Berkeley-ECS method is accurate [33, 64] and is not restricted to single ionization. It can be implemented directly in the same basis that is used to carry out the integration of the TDSE, irrespective of the number of electrons that are eventually produced. With the supercomputers available today, such an approach is feasible for moderate box sizes but prohibitively expensive for larger problems. Both the projection on scattering states (PSS) and the Berkeley-ECS method overcome some of the limitations of methods based on the use of approximated continuum functions while suffering from some drawbacks of their own.

On the one hand, the Berkeley-ECS method is applicable at energies above the double ionization threshold. On the other hand, the PSS method is more convenient below the double ionization threshold. This is because the single ionization space is only a tiny fraction of the discretized continuum which is apt to represent multiple ionization processes. The calculation of scattering states takes advantage of this reduced state space by employing compact close-coupling representations.

Moreover, the two methods have different scaling properties. While scattering states are computed once and for all, and can thus be applied to the analysis of an arbitrary number of wave packets through the evaluation of a simple scalar product, the time-consuming steps of the Berkeley-ECS method must be repeated each time a wave packet is to be analyzed.

The use of scattering states furthermore permits to monitor and isolate the different channel components of the wave functions during the time evolution, in particular to disentangle individual ionization pathways in pump-probe experiments.

The latter holds, of course, only if scattering states *can* be converted from a basis best suited to their efficient calculation to another one which is best suited to integrate the TDSE. We will show in the following that this is indeed possible.

III. PROPAGATION METHOD

Our computational approach (see [32, 65, 66] for a more detailed description) for solving the time-dependent Schrödinger equation for two-electron systems,

$$i \frac{\partial}{\partial t} \Psi(\mathbf{r}_1, \mathbf{r}_2, t) = H \Psi(\mathbf{r}_1, \mathbf{r}_2, t), \quad (13)$$

is based on a time-dependent close-coupling scheme [67–70] where we expand the angular part of the six-dimensional wave function $\Psi(\mathbf{r}_1, \mathbf{r}_2)$ in coupled spherical harmonics $\mathcal{Y}_{l_1, l_2}^{LM}(\Omega_1, \Omega_2)$.

The interaction of a helium atom with linearly polarized light is described by the Hamiltonian

$$H = H_a + H_{\text{em}}^{l,v} = \frac{\hat{\mathbf{p}}_1^2}{2} + \frac{\hat{\mathbf{p}}_2^2}{2} - \frac{2}{r_1} - \frac{2}{r_2} + \frac{1}{|\mathbf{r}_1 - \mathbf{r}_2|} + H_{\text{em}}^{l,v}, \quad (14)$$

where the interaction with the electromagnetic field in the dipole approximation, $H_{\text{em}}^{l,v}$, is either given in *length* or *velocity* gauge. The gauge independence of the physical observables is a necessary condition for the convergence of the numerical solution.

For the discretization of the radial functions $R_{l_1, l_2}^L(r_1, r_2, t)$, we employ a finite-element discrete-variable representation (FEDVR) [71–73]. We divide the radial coordinates into finite elements in each of which the functions R_{l_1, l_2}^L are represented in a local DVR basis with a corresponding Gauss-Lobatto quadrature to ensure the continuity of the wave function at the element boundaries. This method leads to sparse matrix representations of the differential operators and to a diagonal potential matrix (within quadrature accuracy), enabling efficient parallelization.

For the temporal propagation, we employ the short iterative Lanczos (SIL) method [74–76] with adaptive time-step control. The initial He ground state $1^1\text{S}(1s^2)$ is obtained by relaxing an arbitrary test function in imaginary time. For an initial $2^1\text{S}(1s2s)$ metastable state we directly solve the eigenvalue problem of the field-free Hamiltonian (14) in a small box using the SLEPc library [77].

IV. EXTRACTION OF THE SPECTRUM

The four methods used here to extract the single ionization photoelectron spectrum are: (i) projection of the wave packet on the product of a bound hydrogenic wave function with $Z=2$ and a Coulomb continuum function with $Z=1$; (ii) projection on channel functions obtained from the diagonalization of the total Hamiltonian in the configuration space where one of the two electrons is frozen in an hydrogenic state of the parent ion. Channel functions differ from the products of Coulomb functions because, in the radial region where the bound electron density is not zero, the effective potential felt by the free electron departs from that of a nuclear charge with $Z=1$. Yet, at larger distances, these channel functions converge to phase-shifted Coulomb functions. Therefore, for the purpose of evaluating the absolute value of the projection of an outgoing wave packet, channel functions and pure Coulomb functions are essentially equivalent; (iii) projection on scattering states (PSS) obtained with the B-spline K-matrix method; and (iv) extraction of the partial differential photoelectron distribution with the

Berkeley-ECS method. For double ionization we compare the Berkeley-ECS method with the projection of the wave packet on a symmetrized product of two Coulomb functions with $Z=2$.

Our implementation of the Berkeley ECS method closely follows that of Palacios *et al.* [33, 63], which builds on earlier work reviewed in [78]. We give a brief review here and refer the reader to the original papers for details. The central idea is to solve the inhomogeneous linear system

$$(E - H_a)|\Psi_{\text{sc}}(E)\rangle = |\Psi(t_0)\rangle \quad (15)$$

in the basis used for temporal propagation, using the PETSc package [79]. The scattered wave $\Psi_{\text{sc}}(E)$ is equivalent to the Fourier transform of the time-dependent wave packet from $t = t_0$ to $t = \infty$, and corresponds to the application of the retarded Green's function of the total Hamiltonian on the wave packet,

$$|\Psi_{\text{sc}}(E)\rangle = G^+(E)|\Psi(t_0)\rangle. \quad (16)$$

Purely outgoing boundary conditions are enforced by an exterior complex scaling (ECS) transformation for each of the radial coordinates. As the wave packet at the end of the pulse is a square-integrable function, the asymptotic behavior of the scattered wave can be deduced from the asymptotic form of the Green's function. For single ionization, the amplitude $c_{\alpha E}(t_0)$ can be expressed as [78],

$$c_{\alpha E}(t_0) = \langle \varphi_{\alpha E} | E - H_0 | \Psi_{\text{sc}}(E) \rangle, \quad (17)$$

where $\varphi_{\alpha E}$ is an eigenstate of the reference Hamiltonian H_0 . The latter should contain the monopolar long-range interaction between the fragments to suppress spurious contributions. Using Green's theorem allows one to express the single ionization amplitude as a surface integral in the non-scaled region of space,

$$c_{\alpha E}(t_0) = \frac{1}{2} \int_S (\varphi_{\alpha E} \nabla \Psi_{\text{sc}}(E) - \Psi_{\text{sc}}(E) \nabla \varphi_{\alpha E}) \cdot d\mathbf{S}, \quad (18)$$

where $\nabla = (\nabla_1, \nabla_2)$ is the six-dimensional gradient operator (in the present case of helium). Since the integral (Eq. 18) is evaluated in a radial region far from the atom and $\Psi_{\text{sc}}(E)$ is an outgoing wave packet by construction, it is sufficient that $\varphi_{\alpha E}$ satisfies the same outgoing boundary conditions as the eigenstates of H_0 . Thus, in single ionization, $\varphi_{\alpha E}$ can be taken as the symmetrized product of an ionic bound state and a Coulomb wave with $Z = 1$. For double ionization, a similar expression can be found [63, 78].

The single-ionization scattering states of helium below the double ionization threshold of the atom are computed with the B-spline K-matrix method. B-splines are a convenient tool to accurately represent the radial component of continuum atomic orbitals on a finite interval [80, 81], while the K-matrix method [82] is an L^2 realization of configuration interaction in the continuum

along the lines of Fano's pioneering paper [83]. The K-matrix method has been successfully applied for the single-photoionization spectrum of several atomic and molecular systems [45, 56, 84–86]. We will provide here only a brief description of its implementation for the case of helium (details can be found elsewhere [45, 87]).

A complete set $\psi_{\alpha E}^{\mathcal{P}}$ of stationary eigenfunctions of the field-free Hamiltonian H_a at a given energy E in the single-ionization continuum are sought in the form of a linear combination of partial-wave channel functions $\phi_{\alpha E}$ (PWC's), plus an additional component from a localized (or pseudostate) channel (LC),

$$\psi_{\alpha E}^{\mathcal{P}} = \phi_{\alpha E} + \sum_{\gamma} \sum_{\epsilon} d\epsilon \phi_{\gamma \epsilon} \frac{\mathcal{P}}{E - \epsilon} \mathbf{K}_{\gamma \epsilon, \alpha E}, \quad (19)$$

where the index α runs over the channels which are open at energy E , while the index γ runs over all open and closed channels, including the localized one.

The PWC α is defined by coupling and antisymmetrizing a bound state of the He^+ parent ion with quantum numbers N_{α} and L_{α} and energy E_{α} , to an electron state with angular momentum ℓ_{α} , the radial degree of freedom of which is otherwise unconstrained, to give a state with definite values for the total spin S and angular momentum L .

$$\phi_{\alpha E} = \hat{\mathcal{A}} \Theta_{S\Sigma} \mathcal{Y}_{L_{\alpha} \ell_{\alpha}}^{LM}(\Omega_1, \Omega_2) R_{N_{\alpha} L_{\alpha}}(r_1) \frac{f_{\alpha E}(r_2)}{r_2}, \quad (20)$$

where $\hat{\mathcal{A}}$ is the antisymmetrizer, $\Theta_{S\Sigma}$ is a two-electron spin function, $R_{N_{\alpha} L_{\alpha}}$ is the radial part of the frozen He^+ parent ion state, and $f_{\alpha E}$ the continuum radial function. Asymptotically the $f_{\alpha E}$ are a linear combination of the regular and irregular Coulomb functions with angular momentum ℓ_{α} , energy E , and a phase shift $\delta_{\alpha E}$, determined by the short range behavior of the differential equation for $f_{\alpha E}$, which differs from that of the hydrogenic functions. This results from the deviation of the frozen-core potential from that of a pure Coulomb potential.

The PWCs in (Eq. 19) do not exhaust the state space associated to single ionization, because the set of bound states of the parent ion is not complete, and because the close-coupling expansion (Eq. 19) is truncated. Nevertheless, if all single- and double-ionization closed channels were to be included in the close-coupling expansion, their contribution would decay exponentially at large radii. Therefore, instead of using a complete basis, it is sufficient to include in (Eq. 19) a pseudo-state channel LC that comprises a sufficiently large number of normalized two-electron functions built from localized orbitals, to attain good accuracy.

Equation (19) may be solved for the unknown coefficient matrix \mathbf{K} by requiring $\psi_{\alpha E}^{\mathcal{P}}$ to be an eigenfunction of the complete projected Hamiltonian with eigenvalue E ,

$$\langle \phi_{\beta E'} | E - H_a | \psi_{\alpha E}^{\mathcal{P}} \rangle = 0 \quad \forall \beta, E'. \quad (21)$$

This condition leads to a system of integral equations for \mathbf{K} which can be discretized and solved with standard linear algebra routines. The scattering states with definite spherical symmetry $\psi_{\alpha E}^-$ are then computed as

$$\psi_{\alpha E}^- = \sum_{\beta} \psi_{\beta E}^{\mathcal{P}} \left[\frac{1}{1 - i\pi \mathbf{K}(E)} \right]_{\beta\alpha} e^{-i(\sigma_{\ell\alpha} + \delta_{\alpha} - \ell_{\alpha}\pi/2)}, \quad (22)$$

where $\mathbf{K}_{\alpha\beta}(E) \equiv \mathbf{K}_{\alpha E, \beta E}$ is the on-shell reactance matrix (§7.2.3 in [47]) while $\sigma_{\ell\alpha}$ and δ_{α} are the Coulomb and channel phase shifts, respectively. Finally, the scattering states which correspond to Coulomb plane waves associated to a parent ion in a given state A, are given by

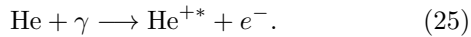
$$\psi_{A, E\Omega\sigma}^- = \sum_{\alpha}^{L_{\alpha}=L_A, N_{\alpha}=N_A} C_{L_A M_A, \ell m}^{LM} C_{\frac{1}{2}\Sigma_A, \frac{1}{2}\sigma}^{S\Sigma} Y_{\ell m}^*(\Omega) \psi_{\alpha E}^-, \quad (23)$$

where L_A , M_A , and Σ_A indicate the parent-ion's angular momentum and spin, Ω and σ indicate the asymptotic photoelectron's direction and spin, and $C_{a\alpha, b\beta}^{c\gamma}$ are Clebsch-Gordan coefficients. The states $\psi_{A, E\Omega\sigma}^-$ are normalized according to

$$\langle \psi_{A, E\Omega\sigma}^- | \psi_{B, E'\Omega'\sigma'}^- \rangle = \delta_{AB} \delta_{\sigma\sigma'} \delta(E - E') \delta(\Omega - \Omega'). \quad (24)$$

V. NUMERICAL EXAMPLES

In this section we present results of alternative extraction methods applied to helium under the action of an ultrashort XUV laser pulse,



Helium is the simplest system that features autoionizing states and excited-threshold openings, hence the differences between the various methods to extract asymptotic observables from an ionization wave packet are particularly transparent in this case.

We carried out two separate simulations, one starting from the ground state 1^1S ($1s^2$) and one starting from the 2^1S ($1s2s$) metastable state (lifetime 19.7 ms [88]) of the atom. A short ($T_{\text{FWHM}}=200$ as), moderately intense ($I_{\text{peak}} = 10^{12}$ W/cm²) Gaussian XUV pulse with carrier frequency $\omega = 2.4$ a.u. and $\omega = 1.65$ a.u., respectively, was employed. In both simulations the energy of the excited component at the end of the pulse was centered on the $N = 2$ threshold in order to populate the 1^1P^o doubly excited states below the threshold. While the oscillator strength for exciting the 1^1P^o doubly excited resonances from the ground state is weak, the excitation probability is strongly enhanced starting from the 2^1S ($1s2s$) singly excited state.

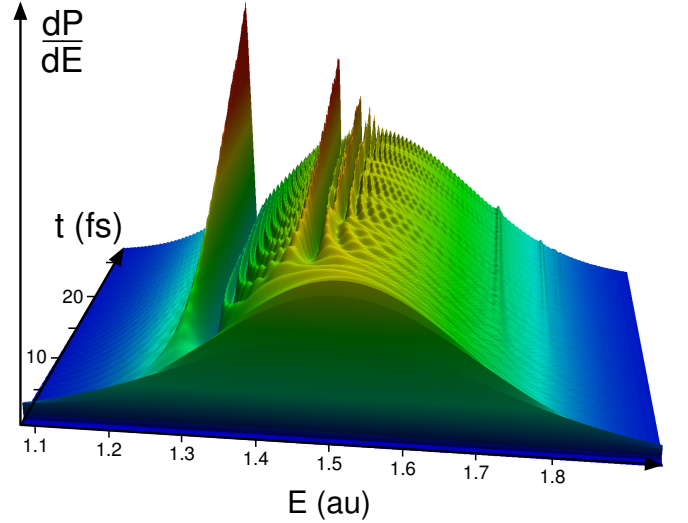


FIG. 2. Total photoelectron spectrum of the wave packet created by the action of a sub-femtosecond pulse on the ground state of the helium atom and computed by projecting the wave packet on products of bound ($Z=2$) and continuum ($Z=1$) Coulomb functions. Since such products are not eigenstates of the field-free Hamiltonian, the spectrum is only approximated and changes with time after the XUV pulse. As the doubly excited states populated by the pulse decay, characteristic Fano profiles build up. See text for more details.

A. Projection on Coulomb functions vs projection on scattering states

In Fig. 2 the square modulus $|\langle 1sE_p | \Psi(t) \rangle|^2$ of the projection on the product of a bound ($Z = 2$) and a continuum ($Z = 1$) Coulomb function of the wave packet starting from the ground state is shown as a function of time. The photoelectron spectrum increases rapidly from zero to a smooth Gaussian profile immediately after the external field is over. At this stage, only the “direct ionization” component is visible, since the duration of the external pulse is much shorter than the lifetime of any of the 1^1P^o metastable states, hence the smoothness of the profile right at the end of the pulse. As time passes, the localized part of the metastable states that were populated by the pulse progressively decay and Fano-like interference features emerge as a consequence. The most prominent among these resonances, seen close to the center of the spectrum, are those converging to the $N=2$ threshold and correspond mostly to the sp_n^+ series of the 1^1P^o autoionizing states [89]. Three major features of this time-dependent spectrum are to be noted. First, each resonance peak takes a long time to reach convergence in comparison to the duration of the laser pulse. Second, decaying resonances give rise to quantum beats due to the interference between the direct and the delayed electron emission [90–92]. Such beats in the time domain are observable when the wave packet is probed at finite times, e.g. by a pump-probe protocol. Third, a whole Rydberg

series of autoionizing states, like the one visible, comprises states with arbitrarily long lifetimes which, with this method, cannot realistically ever be spectrally resolved. A close-up of the spectrum near the $sp_2^+ 1P^o$ (or $2s2p$) resonance (Fig. 3) shows the evolution of the photoelectron spectrum as a function of time determined by projection on the product of Coulomb functions and the asymptotic ($t \rightarrow \infty$) limit of the Fano profile obtained by projecting the wave packet immediately after the end of the pulse on the $\psi_{1sE_p}^-$ scattering states. The scattering states account automatically for the time evolution of the full wave packet to infinity and no free propagation beyond the end of the pulse is required. In turn, quantum beats occurring at finite time are not visible in the PSS method as it projects into the asymptotic future. When the projection is made on scattering states, the propagation can be carried out in a box as small as 200 Bohr radii sufficient to contain the wave packet close to the end of the pulse. This is to be contrasted with the spectrum obtained by the projection on the product of Coulomb functions that has still not reached the asymptotic limit even though the box is an order of magnitude larger in size. The spectrum obtained by projection onto partial-wave channel functions with a frozen core (method (ii) in section IV) yields results very close to the projection onto Coulomb functions (Fig. 3) and will, therefore, not be separately discussed in the remainder of the paper.

B. Conversion of B-spline close-coupling functions to the FEDVR basis

Table I compares the energies of $1S^e$, $1P^o$, and $1D^e$ helium Rydberg states with principal quantum number n for the outer electron up to $n=6$, obtained by diagonalizing the full configuration interaction Hamiltonian of helium built in either the FEDVR or the B-spline basis. The FEDVR basis comprised eleven functions per finite element. The width of the first element was 2 a.u. and increased linearly to 4.0 a.u. within the first 5 finite elements. The grid extensions were 28 a.u. for one radial coordinate and 156 a.u. for the other. The B-spline basis comprised spline functions of order $k=8$ [93] defined on a non-uniform grid of nodes, optimized at small radii to optimize the representation of the ground state of the helium atom, and with an asymptotic spacing between consecutive nodes of 0.5 a.u. up to a maximum radius of 800 a.u.. For both the FEDVR and the B-spline basis, the maximum orbital angular momentum $\ell_{max}=4$ (which suffices for the present comparison between methods) was used. The very good agreement between the two approaches for the Rydberg spectrum indicates that the wave functions in the two bases are represented at comparable levels of accuracy.

To assess the accuracy with which the wave functions computed in the B-spline basis are converted to the FEDVR basis we computed the norm of the converted Rydberg states $\langle \tilde{\phi}_n | \tilde{\phi}_n \rangle$ as well as their overlap $\langle \phi_n | \tilde{\phi}_n \rangle$

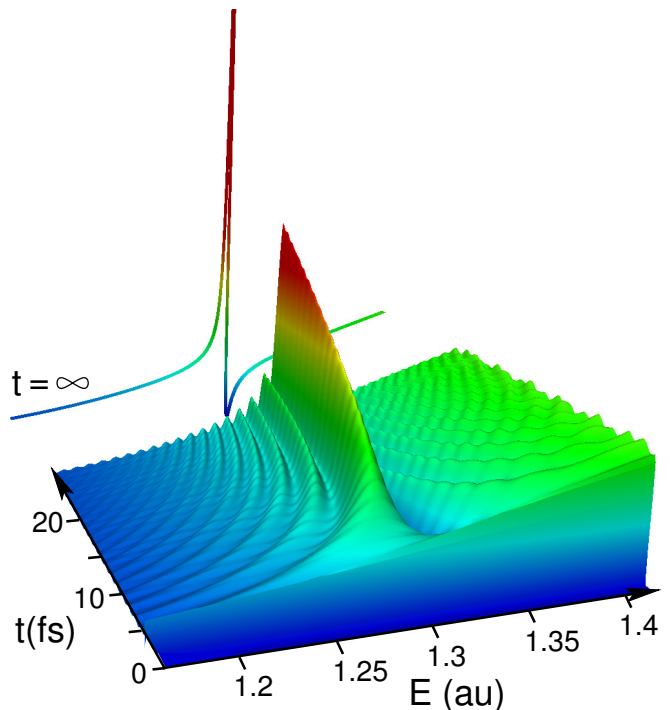


FIG. 3. Close-up of the evolution of the photoelectron spectrum determined by projection on products of Coulomb functions in comparison with the asymptotic Fano profile extracted from the same wave packet by projection onto scattering states immediately after the end of the external pulse.

with the corresponding states computed directly in the FEDVR basis. Both numbers should within the numerical accuracy be close to 1. The errors $\tilde{\delta}_n = 1 - \langle \tilde{\phi}_n | \tilde{\phi}_n \rangle$ and $\delta_n = 1 - \langle \phi_n | \tilde{\phi}_n \rangle$ for the states listed in table I are between 10^{-11} and 10^{-7} (table II).

This confirms the accuracy of the conversion from the B-spline to the FEDVR basis. The error is larger for the ground state than for the excited states because the first finite element is still comparatively wide. This minor discrepancy could be easily fixed by choosing a smaller radial span for the first few finite elements.

C. Comparison between methods

The photoelectron spectrum from the ground state (Fig. 4) is computed (a) by projecting the wave function on products of bound ($Z=2$) and continuum ($Z=1$) Coulomb functions after a lapse of time of 1590 as from the peak of the XUV pulse, (b) by projecting the wave function on the true scattering states of the field-free Hamiltonian, and (c) by extracting it with the Berkeley-ECS method. While the projection on Coulomb functions represents rather well the smooth background spectrum associated to the direct ionization component, it fails to reproduce the sharp features associated to the autoionizing states. The spectra calculated with the PSS

TABLE I. Comparison between the energies of the He Rydberg states with principal quantum number for the outer electron up to $n = 6$, obtained by diagonalizing the Hamiltonian in either the FEDVR (upper value, $R = 156$ a.u.) or the B-spline (lower value, $R=800$ a.u.) basis.

n	$1S^e$	Symmetry $1P^o$	$1D^e$
1	-2.903 5102 -2.903 5164		
2	-2.145 9610 -2.145 9615	-2.123 8231 -2.123 8232	
3	-2.061 2684 -2.061 2685	-2.055 1399 -2.055 1400	-2.055 6203 -2.055 6203
4	-2.033 5852 -2.033 5853	-2.031 0669 -2.031 0669	-2.031 2796 -2.031 2796
5	-2.021 1761 -2.021 1761	-2.019 9046 -2.019 9045	-2.020 0016 -2.020 0016
6	-2.014 5627 -2.014 5627	-2.013 8331 -2.013 8331	-2.013 8981 -2.013 8981

TABLE II. Error in the norm of the bound states translated from the B-spline to the FEDVR basis $\tilde{\delta}_n = 1 - \langle \tilde{\phi}_n | \tilde{\phi}_n \rangle$, and error in the overlap $\delta_n = 1 - \langle \phi_n | \tilde{\phi}_n \rangle$ (see text for details). The notation $[n]$ is a shorthand for 10^{-n} .

n	$1S$		$1P^o$		$1D^e$	
	$\tilde{\delta}_n$	δ_n	$\tilde{\delta}_n$	δ_n	$\tilde{\delta}_n$	δ_n
1	8.0[-7]	8.2[-7]				
2	7.6[-8]	7.8[-8]	7.4[-11]	3.9[-10]		
3	2.4[-8]	2.5[-8]	2.5[-9]	2.7[-9]	3.3[-9]	3.3[-9]
4	1.2[-8]	2.1[-8]	3.0[-9]	1.3[-8]	3.3[-9]	9.8[-9]
5	7.6[-9]	1.7[-8]	3.1[-9]	1.1[-8]	3.3[-9]	1.3[-8]
6	6.1[-9]	1.3[-8]	4.7[-9]	1.6[-8]	4.0[-9]	1.3[-8]

and with the Berkeley-ECS method feature accurately a large number of resonant profiles and are in excellent agreement with each other. We emphasize that the smaller number of resonances appearing in (c) than in (b) is not due to a fundamental limitation of the method but because of the use of a coarser energy grid. Additional insights can be gained from a close-up (Fig. 5a) and a logarithmic presentation of the photoionization probability (Fig. 5b). Fig. 5 highlights two aspects of the performance of the three methods. First, the projection on scattering states and the Berkeley-ECS method are in excellent agreement close to the resonance (Fig. 5a) and down to the smallest probability densities (Fig. 5b). The deviation of the background profile of the spectrum from a parabola at low energies is due to the fact that the Gaussian envelope of the XUV pulse is eventually truncated. Second, the spectrum obtained through the projection on the product of Coulomb functions clearly deviates from the background below -1 a.u., however, only when $P(E)$ is already small ($\lesssim 10^{-4}$ of the direct ionization peak). This error due to the contamination by

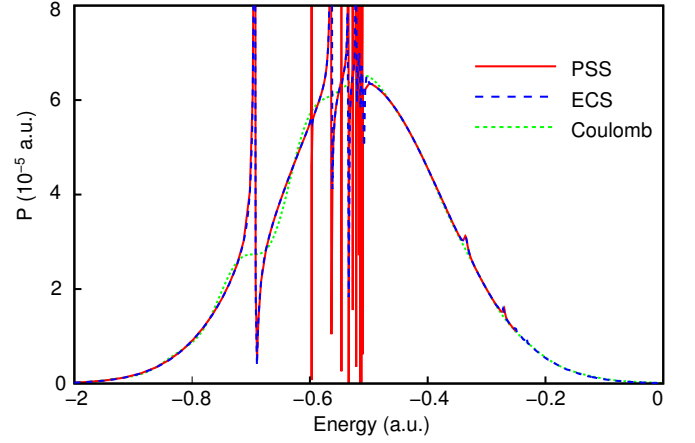


FIG. 4. Photoelectron distribution in the $1s\ 1P^o$ channel resulting from the photoionization of helium from the ground state with an XUV pulse with $\omega = 2.4$ a.u., $I = 10^{12}$ W/cm², and $T_{FWHM}=200$ as. Projection on scattering states (PSS), red solid line; Berkeley-ECS, blue dashed line; projection on the product of Coulomb functions at $t = 1590$ as after the center of the XUV pulse, green dotted line.

doubly excited states is small in the present case since they provide only a minor admixture to the wave packet. When the metastable states have a higher relative weight, however, their spurious effect on the spectrum will be more significant.

The convergence of the DES spectrum as a function of the size of the close-coupling expansion within the PSS is illustrated in Fig. 6. Here, the PSS employs a minimal close-coupling expansion involving the open $N = 2$ channels ($1s\epsilon_p$, $2s\epsilon_p$, $2p\epsilon_s$, and $2p\epsilon_d$) only. Clearly, since the $N=3$ channels are not included, the higher members of the autoionizing Rydberg series converging to the $N=3$ threshold are not reproduced. As a consequence, the spectrum obtained with the PSS deviates from the one obtained with the Berkeley-ECS method at energies higher than -0.3 a.u.. On the other hand, the spectrum below the $N = 3$ threshold is already well converged, i.e. the influence of the closed channels are adequately accounted for. This observation highlights the salient feature of the close-coupling expansion with pseudostates, namely to drastically truncate the representation while still obtaining an accurate representation of the continuum states in any given single-ionization energy region.

The emission spectrum from the metastable $1s2s\ 1S$ excited state of helium ionized by an XUV pulse with central frequency $\omega = 1.65$ a.u. (Fig. 7) reflects the much enhanced role doubly excited states play. Consequently, the errors resulting from projection onto Coulomb functions are more prominent (Fig. 7). Even though the background contribution is semi-quantitatively reproduced, the resonant part which dominates the spectrum is not. Moreover, at low energies the background, if small, is strongly overestimated and as much as two orders of

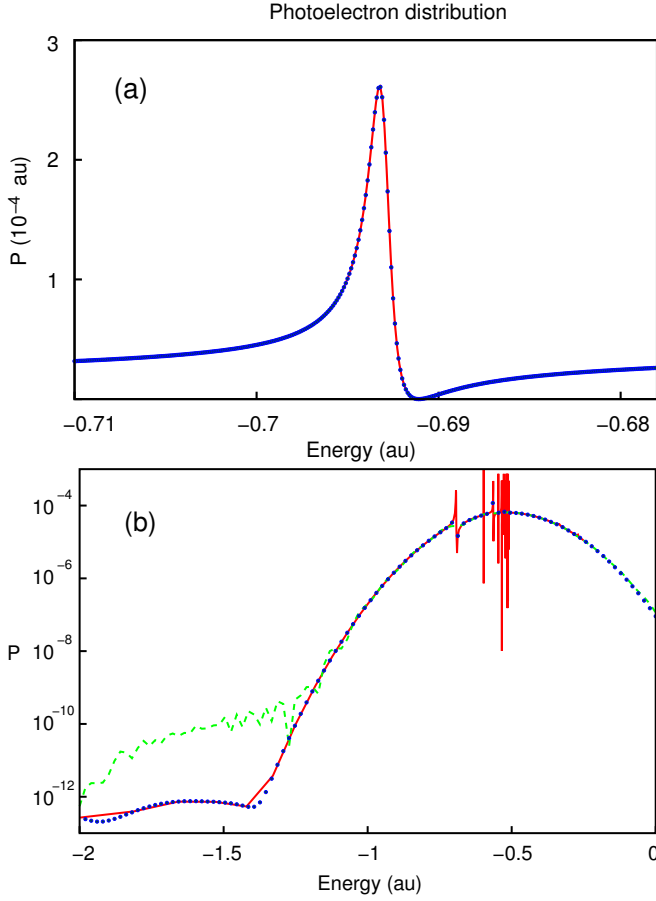


FIG. 5. Photoelectron spectrum as in Fig. 4 with (a) a close-up near the sp_2^+ resonance, and (b) the spectrum on a logarithmic scale to highlight small deviations in the tails of the direct ionization peak.

magnitude larger in absolute terms than in the case of the photoionization from the ground state. The spectra from the other two methods show again an excellent agreement. To complete the comparison between the Berkeley-ECS method and the PSS, we verify whether the two methods predict also the same photoelectron angular distributions. In contrast to energy distributions, angular distributions depend on the relative phases between photoionization amplitudes in different channels as well as on their absolute values. It is thus sufficient to compare the absolute phases of the photoionization amplitudes in the different channels to ascertain whether the angular distribution would also agree. As an example of such a comparison, we present the partial photoelectron distribution in the $2p\epsilon_s$ channel from the $1s2s$ state (Fig. 8a), and the asymptotic phase of the corresponding amplitude in the interaction representation (Fig. 8b). We show here the PSS with two different truncations of the close-coupling expansion, including and excluding the $N = 3$ channels. The agreement in both probability density and phase between the Berkeley-ECS and the PSS is excellent for all open channels included in the expansion.

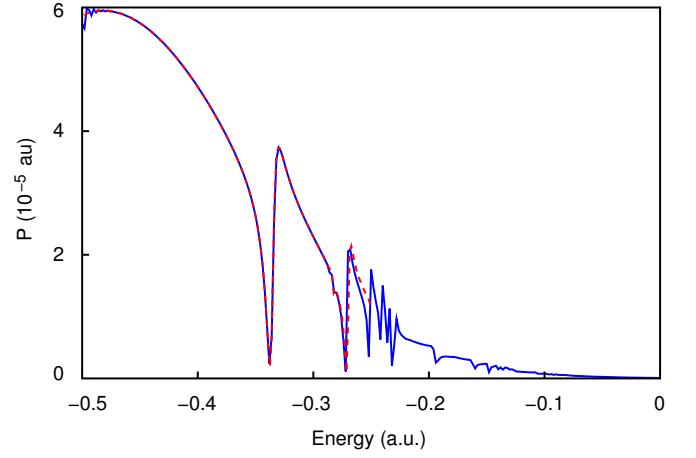


FIG. 6. Photoelectron distribution in the $N = 2 \ ^1P^o$ channel resulting from the photoionization of helium from the ground state with an XUV pulse with $\omega = 2.4$ a.u., $I = 10^{12}$ W/cm², and $T_{\text{FWHM}}=200$ as. PSS: red dashed line; ECS: blue solid line.

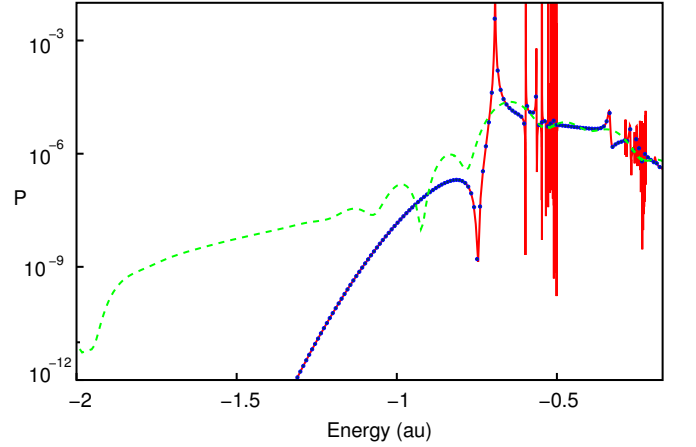


FIG. 7. Photoelectron distribution in the $1s$ channel, following photoionization of the 2^1S metastable state of helium by an XUV pulse with central frequency $\omega = 1.65$ a.u., $I = 10^{12}$ W/cm², and $T_{\text{FWHM}}=200$ as. PSS: red solid line; Berkeley-ECS: blue dotted line; projection onto Coulomb waves: green dashed line.

D. Double ionization spectra

To complete our comparison for the applicability and validity of alternative methods we analyze the continuum components of a correlated wave packet for the doubly ionized part of the spectrum caused by two-photon absorption of the previously used Gaussian XUV pulse with $T_{\text{FWHM}}=200$ as and a carrier frequency $\omega = 2.4$ a.u. from the helium ground state. In this regime, the PSS is

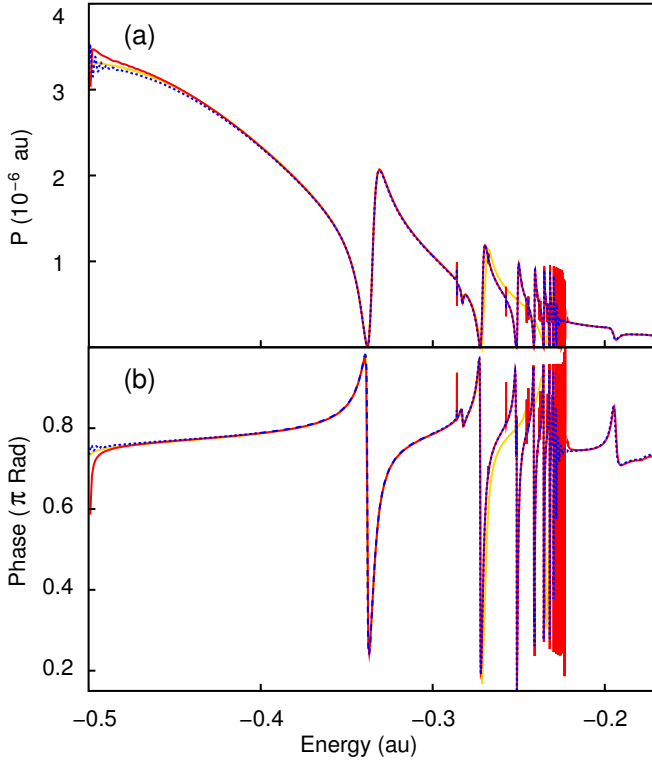


FIG. 8. Partial photoelectron distribution and phase in the $2p\epsilon_s$ channel from photoionization of the $1s2s^1S$ state of helium by an XUV pulse with $\omega = 1.65$ a.u., $I = 10^{12}$ W/cm², and $T_{\text{FWHM}}=200$ as. Three different extraction methods are compared: PSS with a close coupling basis which includes the $N=2$ (dark yellow solid line) and $N=3$ channels (red thick solid line); Berkeley-ECS method (blue dashed line). (a) photoemission probability density P , (b) asymptotic phase of the photoelectron amplitude.

not applicable because of the lack of accurate scattering states for the double continuum. However, the Berkeley-ECS method is able to impose the correct boundary conditions and obtain the asymptotic spectral information of a doubly ionized wave packet directly after the completion of the laser pulse. The projection of the wave packet on an uncorrelated, symmetrized product of two Coulomb functions with $Z = 2$ is straightforward. However, it requires the propagation of the wave packet to large distances in order to control and minimize the error due to the neglect of the electron-electron interaction. In practice this yields accurate results as long as the box and angular momentum basis are large enough to correctly represent the wave function at the time of projection. We compare the singly differential photoelectron spectrum with the prominent two peaks of a sequential two-photon double ionization process. The projection onto Coulomb waves 7500 as after the peak of the pulse shows excellent agreement with the spectrum obtained by the Berkeley-ECS method using the wave packet immediately after the conclusion of the pulse

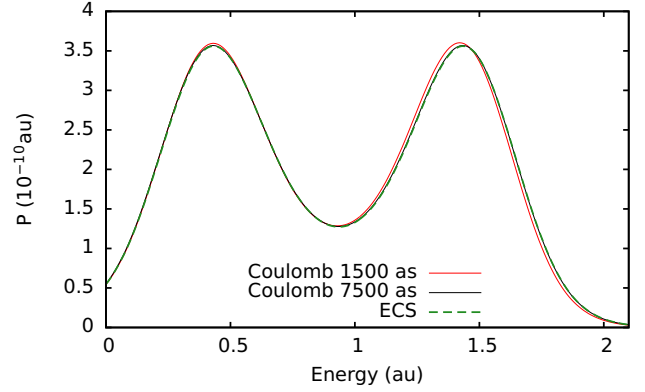


FIG. 9. Singly differential photoelectron distribution after two-photon double ionization of helium by a sub-femtosecond XUV pulse ($\omega = 2.4$ a.u., $I = 10^{12}$ W/cm², and $T_{\text{FWHM}}=200$ as). Two different extraction methods are compared: projection on products of Coulomb functions with $Z = 2$ performed 1500 as (red solid line) and 7500 as (black solid line) after the peak of the XUV pulse and the Berkeley-ECS method (green dashed line) for a computational box with $R = 244$ a.u. performed 1500 as after the peak of the XUV pulse.

(Fig. 9). In fact, virtually the same level of agreement is already reached for considerably smaller propagation times before the projection (not shown). Even projection directly after the conclusion of the field (1500 as after the peak of the XUV pulse, red line in Fig. 9) gives very similar results. We also find very good agreement for the angular distributions, e.g. for the energy-integrated conditional angular emission probability for one electron when the other electron is ejected along the laser polarization axis (Fig. 10a). The remaining small residual differences between the two methods can be understood by inspecting their respective convergence behaviour: The projection on Coulomb functions becomes more accurate when the electrons are propagated further apart before the spectral analysis is performed, provided the partial wave expansion of the wave function covers enough angular momenta to accurately describe the motion of the free electrons. For the present case convergence is reached for propagation times of about 7500 as after the peak of the XUV pulse (see the solid lines in Fig. 10b). The extension of the computational box for the transformation to the spectral domain (i.e. the solution of Eq. 15) and for the surface integral (cf. Eq. 18) influences the quality of the results. Thus, for accurate angular distributions comparably large radial boxes are also required for the Berkeley-ECS method (see the dashed lines in Fig. 10b). The convergence behaviour of the two methods is linked: their results for the angular distributions agree when the extraction radius of the Berkeley-ECS method roughly equals the position of the (relevant parts) of the wave packet at the time of projection on the Coulomb functions (compare solid and dashed lines in Fig. 10b). Thus,

for larger ECS boxes even the small differences to the (converged) Coulomb projection in Fig. 10a would vanish. For both methods the convergence for the angular distributions is considerably slower than for the energy spectra, especially where both electrons are emitted in the same direction (Fig. 10b).

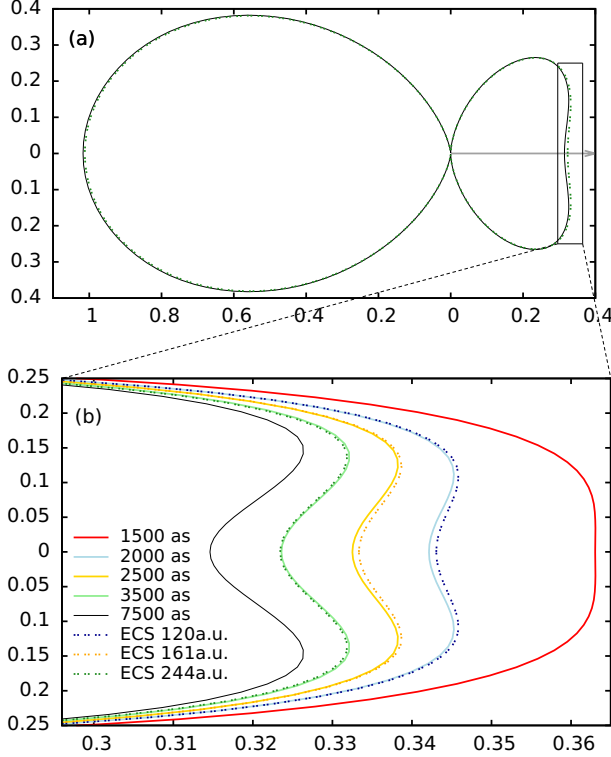


FIG. 10. Conditional angular distribution for one electron emitted in the laser polarization axis [grey arrow in (a)] and integrated over both electron energies after two-photon double ionization of helium by a sub-femtosecond XUV pulse ($\omega = 2.4$ a.u., $I = 10^{12}$ W/cm², and $T_{\text{FWHM}} = 200$ as). Two different extraction methods are compared (a): projection on products of Coulomb functions with $Z = 2$ performed 7500 as (solid black line) after the peak of the XUV pulse and the Berkeley-ECS method (dashed green line) for an extraction radius of $R = 244$ a.u. performed 1500 as after the peak of the XUV pulse. In (b) a close-up of the emission of the two electrons in the same direction is shown. The different lines illustrate the convergence of the Berkeley-ECS method as a function of the extraction radius (dashed lines) and the Coulomb projection as a function of the propagation time (solid lines). The two techniques agree when the extraction radius of the Berkeley-ECS method approximately equals the position of the (relevant parts) of the wave packet at the time of projection on the Coulomb functions, see text. In both cases, the partial wave expansion of the wave function includes angular momenta up to $l_1 = l_2 = 15$.

VI. CONCLUSIONS

We have analyzed and evaluated different methods to extract the continuum component of a correlated multi-electron wave function in helium obtained from the solution of the time-dependent Schrödinger equation. Each of the three methods investigated, the projection onto Coulomb continuum states, the projection onto exact scattering states (PSS), and the Berkeley-ECS method feature both advantages and disadvantages depending on the energy range of interest, the required box size, and whether single or double ionization distributions are desired. Below the double ionization threshold, methods to extract photoelectron spectra that are based on the projection on approximated continuum channels such as Coulomb continuum functions work well when no resonances are significantly populated, but become inapplicable when spectral regions in the vicinity of narrow resonances, are populated. These methods converge extremely slowly, in particular close to thresholds when the wave packet requires long times to reach the asymptotic region. In contrast, remarkably good agreement between the PSS and the Berkeley-ECS method is observed. This finding suggests an efficient way of monitoring the composition of a complex wave packet ψ in the single-ionization channels below the double ionization threshold. Since the scattering states can be computed separately, once and for all, in an adapted basis, the extraction of the expansion coefficients of ψ requires only the calculation of a simple scalar product. Moreover, in contrast to the method based on exterior complex scaling, it opens the way to isolate portions of the wave packet by constructing projections onto specific pre-selected channels. Our current implementation exploits the fact that correlated single-ionization multi-channel scattering states of helium computed on a B-spline basis can be accurately translated to a FEDVR basis in which the wave packet propagation is performed. Such an approach could be extended to alternative methods to accurately compute multi-channel scattering states for atoms and molecules (for example the R-matrix method) in order to extract the wave packet information following the integration of the TDSE on a grid. Above the double ionization threshold, the PSS becomes inapplicable while the Berkeley-ECS method agrees well with projection onto Coulomb functions provided the computational box is sufficiently large and the wave packet is propagated into the asymptotic region.

ACKNOWLEDGMENTS

This work was supported by the MICINN project number FIS2010-15127, the Göran Gustafsson Foundation, the Swedish science research council (VR), the European COST Action CM0702, and the FWF-Austria, Grant No. P21141-N16, P23359-N16. The computational results presented have also been achieved in part using

the Vienna ScientificCluster (VSC). The authors thank Dr. Alicia Palacios for fruitful discussions. JF acknowl-

edges support from the NSF through a grant to ITAMP. R. P. acknowledges support by the TU Vienna Doctoral Program Functional Matter.

-
- [1] G. Sansone, L. Poletto, and M. Nisoli, *Nature Photonics* (Sep. 2011), ISSN 1749-4885, doi:“bibinfo doi 10.1038/nphoton.2011.167”, <http://www.nature.com/doi/doi/10.1038/nphoton.2011.167>
 - [2] B. W. J. McNeil and N. R. Thompson, *Nature Photonics* **4**, 814 (2010)
 - [3] a. D. Shiner, B. E. Schmidt, C. Trallero-Herrero, H. J. Wörner, S. Patchkovskii, P. B. Corkum, J.-C. Kieffer, F. Légaré, and D. M. Villeneuve, *Nature Physics* **7**, 464 (2011), ISSN 1745-2473, <http://dx.doi.org/10.1038/nphys1940>
 - [4] M. Schultze, M. Fiess, N. Karpowicz, J. Gagnon, M. Korbman, M. Hofstetter, S. Neppl, A. L. Cavalieri, Y. Komninos, T. Mercouris, C. A. Nicolaides, R. Pazourek, S. Nagele, J. Feist, J. Burgdörfer, A. M. Azzeer, R. Ernstorfer, R. Kienberger, U. Kleineberg, E. Goulielmakis, F. Krausz, and V. S. Yakovlev, *Science* **328**, 1658 (2010)
 - [5] O. Smirnova, Y. Mairesse, S. Patchkovskii, N. Dudovich, D. M. Villeneuve, P. B. Corkum, and M. Y. Ivanov, *Nature* **460**, 972 (Aug. 2009), ISSN 1476-4687, <http://www.ncbi.nlm.nih.gov/pubmed/19626004>
 - [6] S. Haessler, J. Caillat, W. Boutu, C. Giovanetti-Teixeira, T. Ruchon, T. Auguste, Z. Diveki, P. Breger, A. Maquet, B. Carré, R. Taïeb, and P. Salières, *Nature Physics* **6**, 200 (2010), ISSN 1745-2473, <http://dx.doi.org/10.1038/nphys1511>
 - [7] J. Feist, S. Nagele, C. Ticknor, B. I. Schneider, L. A. Collins, and J. Burgdörfer, *Phys. Rev. Lett.* **107**, 093005 (2011)
 - [8] J. Caillat, A. Maquet, S. Haessler, B. Fabre, T. Ruchon, P. Salières, Y. Mairesse, and R. Taïeb, *Phys. Rev. Lett.* **106**, 093002 (2011)
 - [9] K. Klünder, J. M. Dahlström, M. Gisselbrecht, T. Fordell, M. Swoboda, D. Guénot, P. Johnsson, J. Caillat, J. Mauritsson, A. Maquet, R. Taïeb, and A. L’Huillier, *Phys. Rev. Lett.* **106**, 143002 (2011)
 - [10] A. I. Kuleff and L. S. Cederbaum, *Phys. Rev. Lett.* **106**, 053001 (Jan. 2011), ISSN 0031-9007, <http://link.aps.org/doi/10.1103/PhysRevLett.106.053001>
 - [11] T. Remetter, P. Johnsson, J. Mauritsson, K. Varjú, F. Lépine, E. Gustafsson, M. F. Kling, J. I. Khan, R. López-Martens, K. J. Schafer, M. J. J. Vrakking, and A. L’Huillier, *Nature Physics* **2**, 323 (2006)
 - [12] J. Mauritsson, P. Johnsson, E. Mansten, M. Swoboda, T. Ruchon, A. L’Huillier, and K. J. Schafer, *Phys. Rev. Lett.* **100**, 073003 (2008)
 - [13] J. Feist, S. Nagele, R. Pazourek, E. Persson, B. I. Schneider, L. A. Collins, and J. Burgdörfer, *Phys. Rev. Lett.* **103**, 063002 (Aug. 2009), ISSN 0031-9007, <http://link.aps.org/doi/10.1103/PhysRevLett.103.063002>
 - [14] L. Argenti and E. Lindroth, *Phys. Rev. Lett.* **105**, 053002 (Jul. 2010), ISSN 0031-9007, <http://link.aps.org/doi/10.1103/PhysRevLett.105.053002>
 - [15] G. Sansone, F. Kelkensberg, J. F. Pérez-Torres, F. Morales, M. F. Kling, W. Siu, O. Ghafur, P. Johnsson, M. Swoboda, E. Benedetti, F. Ferrari, F. Lépine, J. L. Sanz-Vicario, S. Zherebtsov, I. Znakovskaya, A. L’Huillier, M. Y. Ivanov, M. Nisoli, F. Martín, and M. J. J. Vrakking, *Nature* **465**, 763 (Jun. 2010), ISSN 0028-0836, <http://www.nature.com/doi/doi/10.1038/nature09084>
 - [16] F. Kelkensberg, W. Siu, J. F. Pérez-Torres, F. Morales, G. Gademann, A. Rouzée, P. Johnsson, M. Lucchini, F. Calegari, J. L. Sanz-Vicario, F. Martín, and M. J. J. Vrakking, *Phys. Rev. Lett.* **107**, 043002 (2011)
 - [17] B. Fischer, M. Kremer, T. Pfeifer, B. Feuerstein, V. Sharma, U. Thumm, C.-D. Schröter, R. Moshhammer, and J. Ullrich, *Phys. Rev. Lett.* **105**, 223001 (Nov. 2010), ISSN 0031-9007, <http://link.aps.org/doi/10.1103/PhysRevLett.105.223001>
 - [18] M. Krüger, M. Schenk, and P. Hommelhoff, *Nature* **475**, 78 (Jul. 2011), ISSN 0028-0836, <http://www.nature.com/doi/doi/10.1038/nature10196>
 - [19] Y. Jiang, A. Rudenko, O. Herrwerth, L. Foucar, M. Kurka, K.-U. Kühnel, M. Lezius, M. F. Kling, J. van Tilborg, A. Belkacem, K. Ueda, S. Düsterer, R. Treusch, C.-D. Schröter, R. Moshhammer, and J. Ullrich, *Phys. Rev. Lett.* **105**, 263002 (Dec. 2010), ISSN 0031-9007, <http://link.aps.org/doi/10.1103/PhysRevLett.105.263002>
 - [20] F. H. M. Faisal, *Theory of Multiphoton Processes* (Plenum Press, New York, 1987)
 - [21] G. Sansone, E. Benedetti, F. Calegari, C. Vozzi, L. Avaldi, R. Flammini, L. Poletto, P. Villoresi, C. Altucci, R. Velotta, S. Stagira, S. De Silvestri, and M. Nisoli, *Science* **314**, 443 (2006)
 - [22] E. Goulielmakis, M. Schultze, M. Hofstetter, V. S. Yakovlev, J. Gagnon, M. Uiberacker, A. Aquila, E. M. Gullikson, D. T. Attwood, R. Kienberger, F. Krausz, and U. Kleineberg, *Science* **320**, 1614 (2008)
 - [23] P. G. Burke, P. Francken, and C. J. Joachain, *J. Phys. B: At. Mol. Opt. Phys.* **24**, 761 (1991)
 - [24] E. S. Smyth, J. S. Parker, and K. T. Taylor, *Comp. Phys. Commun.* **114**, 1 (1998)
 - [25] G. Lagmago Kamta and A. F. Starace, *Phys. Rev. A* **65**, 053418 (2002)
 - [26] S. Laulan and H. Bachau, *Physical Review A* **69**, 033408 (Mar. 2004), ISSN 1050-2947, <http://link.aps.org/doi/10.1103/PhysRevA.69.033408>
 - [27] J. L. Sanz-Vicario, H. Bachau, and F. Martín, *Phys. Rev. A* **73**, 033410 (2006)
 - [28] X.-m. Tong, K. Hino, and N. Tushima, *Phys. Rev. A* **74**, 031405(R) (Sep. 2006), ISSN 1050-2947, <http://link.aps.org/doi/10.1103/PhysRevA.74.031405>
 - [29] E. Fomouou, G. Lagmago Kamta, G. Edah, and B. Piraux, *Phys. Rev. A* **74**, 063409 (2006)
 - [30] P. Lambropoulos and L. A. A. Nikolopoulos, *New J. Phys.* **10**, 025012 (2008)
 - [31] M. A. Lysaght, P. G. Burke, and H. W. van der Hart, *Phys. Rev. Lett.* **101**, 253001 (2008)

- [32] J. Feist, S. Nagele, R. Pazourek, E. Persson, B. I. Schneider, L. A. Collins, and J. Burgdörfer, *Phys. Rev. A* **77**, 043420 (Apr. 2008), ISSN 1050-2947, <http://link.aps.org/doi/10.1103/PhysRevA.77.043420>
- [33] A. Palacios, T. N. Rescigno, and C. W. McCurdy, *Phys. Rev. A* **77**, 032716 (Mar. 2008), ISSN 1050-2947, <http://link.aps.org/doi/10.1103/PhysRevA.77.032716>
- [34] R. Nepstad, T. Birkeland, and M. Førrø, *Phys. Rev. A* **81**, 063402 (Jun. 2010), ISSN 1050-2947, <http://link.aps.org/doi/10.1103/PhysRevA.81.063402>
- [35] A. T. J. B. Eppink and D. H. Parker, *Rev. Sci. Instrum.* **68**, 3477 (1997)
- [36] J. Ullrich, R. Moshhammer, A. Dorn, R. D. Dörner, L. P. H. Schmidt, and H. Schmidt-Böcking, *Rep. Prog. Phys.* **66**, 1463 (2003)
- [37] E. Goulielmakis, Z.-H. Loh, A. Wirth, R. Santra, N. Rohringer, V. S. Yakovlev, S. Zherebtsov, T. Pfeifer, A. M. Azzeer, M. F. Kling, S. R. Leone, and F. Krausz, *Nature* **466**, 739 (Aug. 2010), ISSN 0028-0836, <http://www.nature.com/doi/10.1038/nature09212>
- [38] L. A. A. Nikolopoulos, T. K. Kjeldsen, and L. B. Madsen, *Phys. Rev. A* **75**, 1 (Jun. 2007), ISSN 1050-2947, <http://link.aps.org/doi/10.1103/PhysRevA.75.063426>
- [39] T. K. Kjeldsen, L. B. Madsen, and J. Hansen, *Phys. Rev. A* **74**, 1 (Sep. 2006), ISSN 1050-2947, <http://link.aps.org/doi/10.1103/PhysRevA.74.035402>
- [40] L. B. Madsen, L. A. A. Nikolopoulos, T. K. Kjeldsen, and J. Fernández, *Phys. Rev. A* **76**, 063407 (2007)
- [41] C. W. McCurdy, M. Baertschy, and T. N. Rescigno, *J. Phys. B: At. Mol. Opt. Phys.* **37**, R137 (Sep. 2004), ISSN 0953-4075, <http://stacks.iop.org/0953-4075/37/i=17/a=R01?key=crossref.2b47a7395a8201d53f3f3b2697689fbc>
- [42] A. Palacios, H. Bachau, and F. Martín, *Phys. Rev. Lett.* **96**, 143001 (2006)
- [43] A. K. Kazansky, P. Selles, and L. Malegat, *Phys. Rev. A* **68**, 052701 (Nov. 2003), ISSN 1050-2947, <http://link.aps.org/doi/10.1103/PhysRevA.68.052701>
- [44] J. Fernández and L. B. Madsen, *J. Phys. B: At. Mol. Opt. Phys.* **42**, 085602 (Apr. 2009), ISSN 0953-4075, <http://stacks.iop.org/0953-4075/42/i=8/a=085602?key=crossref.dd08a12f4c22eab66e8a422af0f4b69d>
- [45] L. Argenti and R. Moccia, *J. Phys. B: At. Mol. Opt. Phys.* **39**, 2773 (2006)
- [46] M. Brauner, J. S. Briggs, and H. Klar, *J. Phys. B: At. Mol. Opt. Phys.* **22**, 2265 (1989)
- [47] R. G. Newton, *Scattering Theory of Waves and Particles* (McGraw-Hill, New York, 1966)
- [48] M. Reed and B. Simon, *Methods of Modern Mathematical Physics. III: Scattering Theory* (Academic Press, Inc., San Diego, California, US, 1979)
- [49] J. Feist, R. Pazourek, S. Nagele, E. Persson, B. I. Schneider, L. A. Collins, and J. Burgdörfer, *J. Phys. B: At. Mol. Opt. Phys.* **42**, 134014 (Jul. 2009), ISSN 0953-4075, <http://stacks.iop.org/0953-4075/42/i=13/a=134014?key=crossref.33d207a1a5c6fbcd2a628113f2a0a957>
- [50] E. Fomouou, P. Antoine, H. Bachau, and B. Piroux, *New J. Phys.* **10**, 025017 (2008)
- [51] G. Breit and H. A. Bethe, *Phys. Rev.* **93**, 888 (Feb 1954), <http://link.aps.org/doi/10.1103/PhysRev.93.888>
- [52] S. Altshuler, *Il Nuovo Cimento* (1955-1965) **3**, 246 (1956)
- [53] J. T. Broad and W. P. Reinhardt, *Phys. Rev. A* **14**, 2159 (1976)
- [54] M. L. Du and A. Dalgarno, *Phys. Rev. A* **43**, 3474 (1991)
- [55] I. Bray, D. A. Konovalov, and I. E. McCarthy, *Phys. Rev. A* **43**, 1301 (1991)
- [56] R. Moccia and P. Spizzo, *Phys. Rev. A* **43**, 2199 (1991)
- [57] I. Sánchez and F. Martín, *Phys. Rev. A* **44**, 13(R) (1992)
- [58] P. G. Burke, *R-Matrix Theory of Atomic Collisions* (Springer-Verlag, Heidelberg, 2011)
- [59] W. Vanroose, J. Broeckhove, and F. Arickx, *Phys. Rev. Lett.* **88**, 010404 (Dec. 2002), ISSN 0031-9007, <http://link.aps.org/doi/10.1103/PhysRevLett.88.010404>
- [60] I. Cacelli, V. Carravetta, A. Rizzo, and M. Roberto, *Phys. Rep.* **205**, 283 (1991)
- [61] F. Martin, *Phys. Rev. A* **48**, 331 (1993)
- [62] M. Venuti, P. Decleva, and A. Lisini, *J. Phys. B: At. Mol. Opt. Phys.* **29**, 5315 (1996)
- [63] A. Palacios, C. W. McCurdy, and T. N. Rescigno, *Phys. Rev. A* **76**, 043420 (Oct. 2007), ISSN 1050-2947, <http://link.aps.org/doi/10.1103/PhysRevA.76.043420>
- [64] A. Palacios, T. N. Rescigno, and C. W. McCurdy, *Phys. Rev. A* **79**, 033402 (Mar. 2009), ISSN 1050-2947, <http://link.aps.org/doi/10.1103/PhysRevA.79.033402>
- [65] J. Feist, *Two-photon double ionization of helium*, Ph.D. thesis, Vienna Univ. of Technology (2009)
- [66] B. I. Schneider, J. Feist, S. Nagele, R. Pazourek, S. X. Hu, L. A. Collins, and J. Burgdörfer, in *Quantum Dynamic Imaging*, CRM Series in Mathematical Physics, edited by A. D. Bandrauk and M. Ivanov (Springer, 2011) Chap. 10
- [67] J. Colgan and M. S. Pindzola, *Phys. Rev. Lett.* **88**, 173002 (2002)
- [68] S. Laulan and H. Bachau, *Phys. Rev. A* **68**, 013409 (Jul. 2003)
- [69] S. X. Hu, J. Colgan, and L. A. Collins, *J. Phys. B* **38**, L35 (2005)
- [70] M. S. Pindzola, F. Robicheaux, S. D. Loch, J. C. Berengut, T. Topcu, J. Colgan, M. Foster, D. C. Griffin, C. P. Ballance, D. R. Schultz, T. Minami, N. R. Badnell, M. C. Witthoef, D. R. Plante, D. M. Mitnik, J. A. Ludlow, and U. Kleiman, *J. Phys. B* **40**, R39 (2007)
- [71] T. N. Rescigno and C. W. McCurdy, *Phys. Rev. A* **62**, 032706 (2000)
- [72] C. W. McCurdy, D. A. Horner, and T. N. Rescigno, *Phys. Rev. A* **63**, 022711 (2001)
- [73] B. I. Schneider, L. A. Collins, and S. X. Hu, *Phys. Rev. E* **73**, 036708 (2006)
- [74] T. J. Park and J. C. Light, *J. Chem. Phys.* **85**, 5870 (1986)
- [75] E. S. Smyth, J. S. Parker, and K. T. Taylor, *Comput. Phys. Commun.* **114**, 1 (Nov. 1998)
- [76] C. Leforestier, R. H. Bisseling, C. Cerjan, M. D. Feit, R. Friesner, A. Guldberg, A. Hammerich, G. Jolicard, W. Karrlein, H.-D. Meyer, N. Lipkin, O. Roncero, and R. Kosloff, *J. Comp. Phys.* **94**, 59 (1991)
- [77] V. Hernandez, J. E. Roman, and V. Vidal, *ACM Trans. Math. Softw.* **31**, 351 (Sep. 2005)
- [78] C. W. McCurdy, M. Baertschy, and T. N. Rescigno, *J. Phys. B* **37**, R137 (2004)
- [79] S. Balay, J. Brown, K. Buschelman, W. D. Gropp, D. Kaushik, M. G. Knepley, L. C. McInnes, B. F. Smith, and H. Zhang, “PETSc Web page,” (2011)
- [80] H. Bachau, E. Cormier, P. Decleva, J. E. Hansen, and F. Martín, *Rep. Prog. Phys.* **64**, 1815 (2001)
- [81] L. Argenti and R. Colle, *Comp. Phys. Commun.* **180**, 1442 (Sep. 2009), ISSN 00104655, <http://linkinghub.elsevier.com/retrieve/pii/S0010465509000848>

- [82] I. Cacelli, V. Carravetta, A. Rizzo, and R. Moccia, Phys. Rep. **205**, 283 (1991)
- [83] U. Fano, Phys. Rev. **124**, 1866 (1961)
- [84] T. K. Fang and T. N. Chang, Phys. Rev. A **61**, 062704 (2000)
- [85] L. Argenti and R. Moccia, *J. Phys. B: At. Mol. Opt. Phys.* **41**, 035002 (Feb. 2008), ISSN 0953-4075, <http://stacks.iop.org/0953-4075/41/i=3/a=035002?key=crossref.5ab2921b96d1d4c22b002a1e537e96d7>
- [86] L. Argenti and R. Moccia, *J. Phys. B: At. Mol. Opt. Phys.* **43**, 235006 (2010)
- [87] E. Lindroth and L. Argenti, Adv. Q. Chem. **63**, XXX (2012)
- [88] G. W. F. Drake, G. A. Victor, and A. Dalgarno, Phys. Rev. **180**, 25 (1969)
- [89] J. W. Cooper, U. Fano, and F. Prats, Phys. Rev. Lett. **10**, 518 (1963)
- [90] M. Wickenhauser, J. Burgdörfer, F. Krausz, and M. Drescher, *Phys. Rev. Lett.* **94**, 023002 (2005)
- [91] M. Wickenhauser, Burgdörfer, F. Krausz, and M. Drescher, *J. Mod. Opt.* **53**, 247 (Jan. 2006)
- [92] M. Wickenhauser, *Ionization dynamics of atoms in femto- and attosecond pulses*, Ph.D. thesis, Vienna Univ. of Technology (2006)
- [93] H. Bachau, E. Cormier, P. Decleva, J. E. Hansen, and F. Martín, Rep. Prog. Phys. **64**, 1815 (2001)